Chapter 2
Experimental Methods

Crystal Growth

All the oxide compounds listed below were identified with power X-ray diffraction. The orientation of single crystals was confirmed by Laue X-ray photography. Depending on the purpose, they were cut into rectangular shapes using a crystal cutter (for oxides) or razor's edge (for halides).

$CuFeO_2$, $CuFe_{1-x}Al_xO_2$ and $CuFe_{1-x}Ga_xO_2$

Single crystals of $CuFeO_2$, $CuFe_{1-x}Al_xO_2$ ($x = 0.01, 0.02$), and $CuFe_{1-x}Ga_xO_2$ ($x = 0.01, 0.035$) were grown by a floating zone method. As starting materials, powders of Cu_2O, Fe_2O_3, Al_2O_3, and Ga_2O_3 were used. Stoichiometric amounts of powders were mixed, ground, and sintered at 950 °C for 24 h in Ar atmosphere. The obtained polycrystal was pressed into a rod-shape. The single crystal growth was carried out in an infrared radiation furnace, with Ar atmosphere and an upper (lower) zone speed of 1.5 mm/h (3.0 mm/h), respectively. Since $CuFeO_2$ partially decomposes above 1, 180 °C, the first several cm of the crystal includes excess Fe_2O_3. As the growth goes on, composition of the molten zone gradually changes and finally the pure $CuFeO_2$ (or $CuFe_{1-x}Al_xO_2$ / $CuFe_{1-x}Ga_xO_2$) phase becomes stable [1]. Thus, we picked up only the last 5 cm of the obtained crystal. Because the doping of Al or Ga seems to slow down the convergence of crystallographic domains, we checked the single domain nature of each specimen under polarized optical microscope.[1]

[1] To observe the crystallographic domain structure under the polarized optical microscope, we require a flat mirror surface. For this purpose, the specimen of $CuFeO_2$ was polished using Al_2O_3 powder with radius down to 0.3 μm

S. Seki, *Magnetoelectric Response in Low-Dimensional Frustrated Spin Systems*, Springer Theses, DOI: 10.1007/978-4-431-54091-5_2,

$ACrO_2$ (A = Cu, Ag, Li and Na)

Single crystals of $CuCrO_2$ were grown by a Bi_2O_3-flux method. Powders of CuO (4.1 mg) and Cr_2O_3 (3.9 mg) were put into a Pt crucible (50 cc), and then Bi_2O_3-powder was added to fill up about 4/5 of the crucible. To melt the mixture of powders, they were heated in air atmosphere at 1, 280 °C for 24 h. The crucible was cooled slowly (1 °C/h) down to 750 °C, and then done rapidly (150 °C/h) down to the room temperature. By this method, we can obtain plate-shaped $CuCrO_2$ single crystals with widest faces parallel to the (001)-plane. The maximum size of the crystal was $7 \times 4 \times 1.5$ mm.

Polycrystals of $AgCrO_2$, $LiCrO_2$, and $NaCrO_2$ were prepared by solid state reaction from the stoichiometric mixture of Ag, Li_2CO_3, Na_2CO_3 and Cr_2O_3. They were heated at 900 °C for 48 h in O_2, at 1, 200 °C for 24 h in air, and at 1, 100 °C for 30 h in Ar, respectively. Powder x-ray diffraction measurements showed no detectable impurity, except a trace of Ag in $AgCrO_2$ specimen and of Cr_2O_3 in $NaCrO_2$ specimen. They were pressed into rods, sintered with additional heating, and cut into thin plates.

$LiCu_2O_2$ and $NaCu_2O_2$

Single crystals of $LiCu_2O_2$ were grown by a self-flux method. Stoichiometric amounts of Li_2CO_3 and CuO were put into an alumina crucible, and heated up to 1, 100 °C in air atmosphere. They were cooled slowly (2.5 °C/h) down to 930 °C, and then done rapidly (900 °C/h) down to the room temperature. Obtained $LiCu_2O_2$ single crystal is plate-shaped, with widest faces parallel to the (001)-plane. They also frequently possess additional cleavage planes parallel to (210). Due to the $a \sim 2b$ relationship of lattice constants, the fine twin structure with mixing of the a and b-axis domains was observed under a polarized optical microscope [2]. All the measurements on $LiCu_2O_2$ in this thesis were performed for the ab-twinned specimen.[2]

Single crystals of $NaCu_2O_2$, which were grown by a self-flux method [3], were provided by Prof. Keimer's group at Max Planck Institute. Since $NaCu_2O_2$ is relatively sensitive to humidity, the crystal was stored in an evacuated desiccator.

$CuCl_2$, VCl_2, MnI_2 and CoI_2

Single crystals of $CuCl_2$, MnI_2, and CoI_2 were grown by a Bridgeman method. Powder of each compound was sealed into an evacuated quartz tube ($\phi = 15$ mm) with V-shaped end. They were slowly dragged down (2.5 mm/h) through the

[2] With inappropriate conditions, unintensional growth of $LiCu_3O_3$ and/or Li_2CuO_2 was often confirmed. Since they don't have the twin structure as found in $LiCu_2O_2$, unintended phases can be easily distinguished under polarized optical microscope.

temperature gradient (10 °C/cm) produced by two-zone furnace. The temperature of upper (hotter) heater was set 700 °C for $CuCl_2$, 550 °C for CoI_2, and 700 °C for MnI_2, respectively.

Single crystals of VCl_2 were purchased from Mitsuwa Chemical Co., Ltd. They possess flake-like shape with thickness of ∼0.3 mm and widest faces parallel to the (001)-plane, probably grown by the chemical vapor transport method.

Since most of MX_2-type halides are extremely sensitive to the humidity, all the handling of the specimen were performed in an Ar-filled glove box. When we measure these compounds outside of the glove box, whole surface of the specimen was covered by small amount of Apiezon-N grease to shut out the moisture in air.

Magnetic Property Measurement

Magnetization measurement was performed using a SQUID magnetometer.

Dielectric Property Measurement

For dielectric property measurements, silver paste was painted on the parallel surfaces of the specimen as electrodes. We often employed two sets of electrodes to simultaneously measure two orthogonal components of electric polarization vector.

Dielectric Constant

Dielectric constant is deduced using a LCR-meter (Agilent E4980A) in the frequency range of 1 MHz $\sim$ 1 kHz. In general, the relationship among dielectric constant ($\varepsilon^\omega = \varepsilon_1 + i\varepsilon_2$), electric conductivity ($\sigma^\omega = \sigma_1 + i\sigma_2$), and admittance ($Y^\omega$) is given by the following equations.

$$j^\omega = \sigma^\omega \cdot E^\omega \tag{2.1}$$

$$\sigma^\omega = i\omega\varepsilon^\omega \tag{2.2}$$

$$Y^\omega = \sigma^\omega \cdot \frac{S}{l} \tag{2.3}$$

Here, j^ω, E^ω, S, and l represent current density, electric field, area of electrode, and thickness of the specimen, respectively. When the specimen can be considered as a RC-circuit with parallel connection of resistivity R_p and capacitance C_p, its admittance Y^ω can be given as $Y^\omega = (1/R_p) + i\omega C_p$. LCR-meter measures Y^ω,

and displays the values of C_p and $D = 1/(2\pi\omega C_p R_p)$. As a result, ε_1 and ε_2 can be obtained by the following equations.

$$\varepsilon_1 = \frac{C_p l}{S} \tag{2.4}$$

$$\varepsilon_2 = \frac{2\pi l C_p D}{S} \tag{2.5}$$

Electric Polarization

Electric polarization (P) is deduced using an electrometer (Keithley Model 6517A). When the magnitude of P changes as a function of time (t), the rearrangement of surface charge induces polarization current (J).

$$\frac{\mathrm{d}P}{\mathrm{d}t} = j = \frac{J}{S} \tag{2.6}$$

Here, j and S indicate polarization current density and area of electrode. Electrometer can measure the polarization current in an accuracy of sub-pA. To obtain the magnitude of P, we measured J with constant rates of temperature-sweep ($2 \sim 20$ K/min), H-sweep ($50 \sim 131$ Oe/sec), or H-rotation ($0.5° \sim 2°$/sec), and integrated it with time.

To enlarge the population of specific P-domains, the poling electric field ($50 \sim 300$ kV/m) was applied along the appropriate direction in the cooling process and removed just prior to the measurements of polarization current. Without this poling procedure, an equal population of $\pm P$ domains appears and no polarization current can be observed.

Heat Capacity Measurement

Heat capacity was measured using a thermal relaxation method [4]. We assume that the specimen (with heat capacity C and temperature T) and the thermal bath (with temperature T_0) is connected by the wire (with thermal conductivity k), and thermal power P is provided to the specimen via the heater attached to the sample platform[3] (Fig. 2.1). The sample temperature T as a function of time t obeys the following equation.

$$P(t) = k(T - T_0) + C\frac{\mathrm{d}T}{\mathrm{d}t} \tag{2.7}$$

[3] Here, we assume the good thermal contact between the specimen and the sample stage. For this purpose, Apiezon-N grease is used to fix the sample.

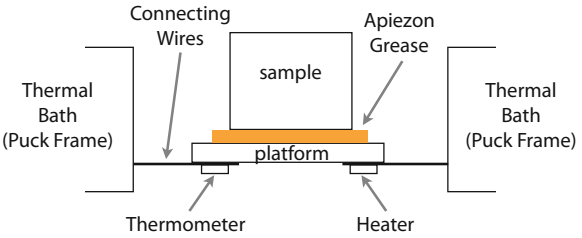

Fig. 2.1 Thermal connections to sample and sample platform [4]

When the heater is switched off (i.e. $P = 0$), the temperature variation between the specimen and heat bath $(T - T_0)$ shows the relaxation behavior.

$$(T - T_0) = (T_1 - T_0)\exp(-t/\tau) \tag{2.8}$$

Here, τ and T_1 represent thermal relaxation time and sample temperature just before the heater is turned off, respectively. The heat capacity C of the specimen can be obtained by the following equation.

$$\tau = C/k \tag{2.9}$$

In reality, C also contains the contribution from the sample platform and thermal grease. Thus, we performed the same measurements with and without the sample, and deduced the pure contribution from the specimen.

Electron Spin Resonance

ESR signal was measured by JEOL JES-FA200 at X-band frequency ($\nu \sim 9.0$ GHz). The experimental setup is illustrated in Fig. 2.2a. The sample sits in a resonant cavity, and microwave radiation with fixed frequency enters via a waveguide. To induce the Zeeman splitting, static magnetic field H is applied perpendicular to the magnetic component of microwave. Electron paramagnetic resonance is observed when the energy gap (Δ) between $m_s = \pm 1/2$ states becomes equal to $h\nu$ (Fig. 2.2b).[4]

$$h\nu = \Delta = g\mu_{\mathbf{B}}H. \tag{2.10}$$

We measured the microwave absorption as a function of H, and deduced the g-value from the magnitude of resonance field. By rotating the specimen within a cavity, the angle-dependence (i.e. anisotropy) of g-value was also investigated.

[4] Here, we assume $CuCl_2$ with $S = 1/2$ as the target compound. To avoid the humidity, the specimen was sealed into a quartz tube filled with Ar-gas.

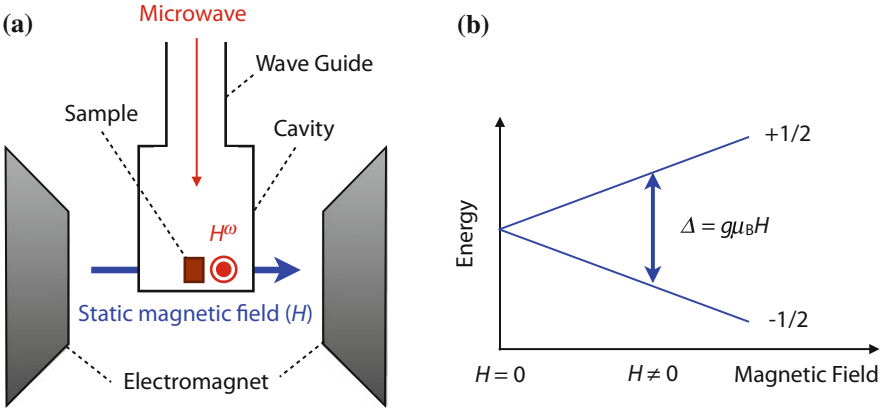

Fig. 2.2 **a** Schematic illustration of the experimental setup for ESR measurement. **b** Zeeman splitting between $m_s = \pm 1/2$ states

Polarized Neutron Scattering

Polarized neutron diffraction study was performed with Polarized Neutron Triple-Axis Spectrometer (PONTA) of ISSP-NSL at JRR-3M. Neutron diffraction is known as one of most powerful experimental methods to determine the magnetic structure in solids. The employment of polarized neutron provides additional sensitivity to the spin-orientation and spin-helicity (clockwise or counter-clockwise manner of spin rotation) of the target compound, which enables more precise characterization of non-collinear magnetic structure.[5]

Figure 2.3 indicates the schematic illustration of experimental setup. We define the scattering vector $\mathbf{Q}$ as $\mathbf{Q} = \mathbf{k}_f - \mathbf{k}_i$, where $\mathbf{k}_i$ and $\mathbf{k}_f$ represent wave vectors of incident and scattered neutrons, respectively. Originally, each incident neutron possesses the random spin direction. Neutron spin orientation ($\mathbf{S}_n$) is aligned by the Heusler (111) monochromator, and the polarized state is sustained by the guide magnetic field applied throughout the neutron beam path. $\mathbf{S}_n$ can be reversed by the "spin-flipper", which is inserted between the specimen and monochromater. The specimen is surrounded by the Helmholtz coil. Since quantization axis of neutron spin is always parallel to the field direction, we can reorient $\mathbf{S}_n$ by controlling the direction of magnetic field (∼10 mT) generated via the Helmholtz coil. Depending on the purpose, we employed two different configurations; $\mathbf{S}_n \perp \mathbf{Q}$ and $\mathbf{S}_n \perp \mathbf{Q}$.

The flipping ratio of polarized to unpolarized neutrons measured at the (2,1,0) nuclear reflection was sufficiently large; 33 for $\mathbf{S}_n \perp \mathbf{Q}$ and 27 for $\mathbf{S}_n \parallel \mathbf{Q}$. The sample was mounted on a sapphire plate in a closed-cycle helium refrigerator, so that the horizontal scattering plane of the spectrometer coincided with the (h k 0) zone. The neutron energy was fixed at 13.47 meV, and only the elastic scattering experiments

[5] For detail, see "LiCu2O2: Correlation Between Spin-Helicity and Electric Polarization Vector".

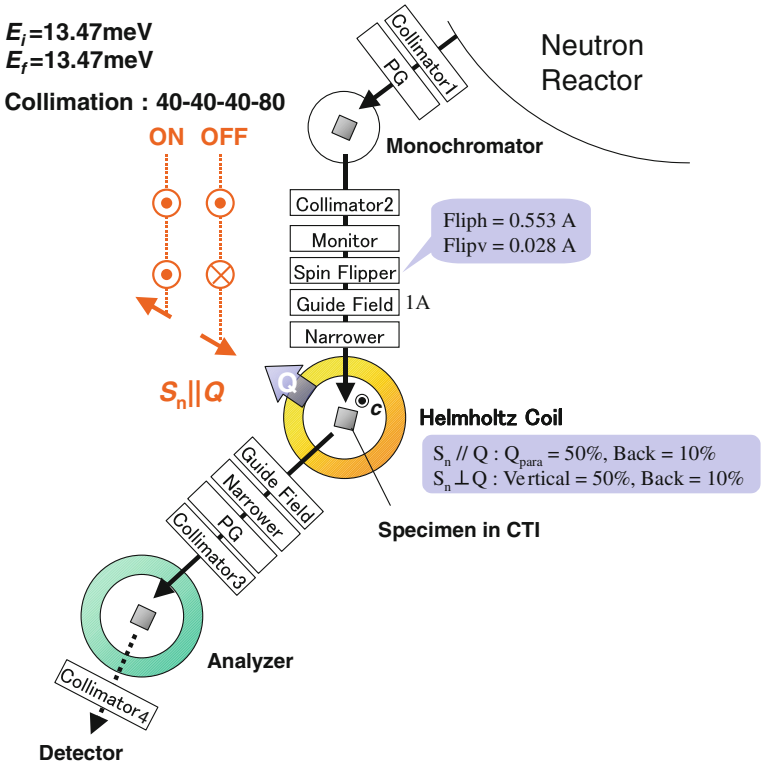

Fig. 2.3 Experimental setup for polarized neutron diffraction study with $\mathbf{S}_n \perp \mathbf{Q}$ condition. *Red arrows* and ON/OFF indicate the spin direction of incident neutron and the state of spin-flipper, respectively

were performed. Pyrolytic graphite (PG) filters were used to eliminate higher harmonic reflections from the monochromator. Collimators (40′-40′-40′-80′) were used to obtain the parallel neutron beam. The size of the specimen ($LiCu_2O_2$) used for the neutron study is 12 mm^2 (*ab* plane) $\times$0.6 mm (*c*-axis). All the data for $LiCu_2O_2$ presented in this thesis were measured on the identical sample.

THz Time-Domain Spectroscopy

We used the terahertz time-domain spectroscopy (THz-TDS) in a transmission geometry to obtain complex refractive index n without using Kramers-Kronig analysis. THz-TDS can easily access the low-energy electrodynamics in solids, with typical frequency range from 0.1 to 3 THz. The lower limit of the measurable frequencies depends on the size of the samples since 0.1 THz corresponds to 3 mm in wave-

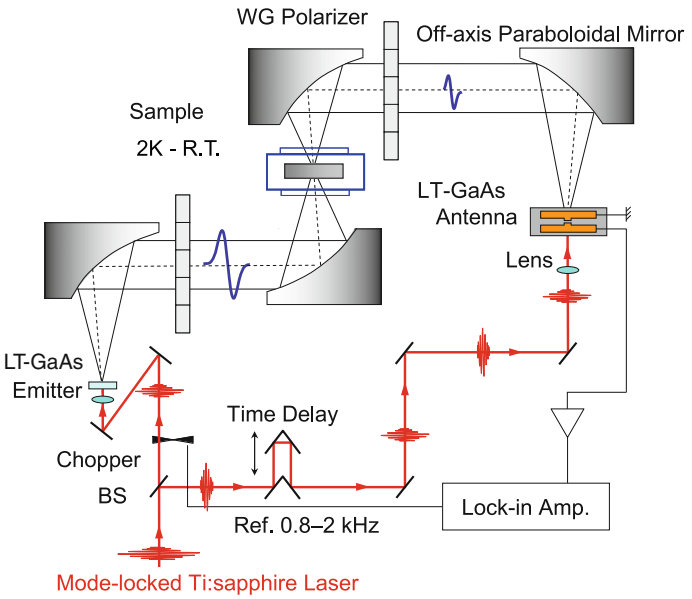

Fig. 2.4 Schematic illustration of the experimental setup for THz time-domain spectroscopy in a transmission geometry. (Adapted with permission from [5], ©2008 APS)

length. The sample was attached to the perforated Cu holder with a diameter of 2.4 ∼ 3.5 mm, which was selected to suitably match the size of the samples.

Figure 2.4 shows the schematic illustration of the experimental setup. For the measurements, we used the photoconducting (PC) sampling technique to obtain terahertz radiation pulse. The femtosecond laser pulses delivered from the mode-locked Ti:sapphire laser were used as a source. The laser pulses were divided by a beam splitter (BS). One was used as the pump and another was used as the gate. The pump pulses were irradiated on the low-temperature-grown GaAs (LT- GaAs) photoconducting device coupled with a dipole antenna to induce the terahertz radiation. The wire grid (WG) polarizers were inserted in between off-axis paraboloidal mirrors to obtain the linear polarization. The polarized terahertz pulse was focused on the sample by off-axis paraboloidal mirrors. The cryostat was placed within the box filled with dry N_2-gas to eliminate the absorption of water. The gate pulses were introduced to the LT-GaAs antenna after the appropriate time delay. The pump pulses were mechanically chopped and the photocurrent induced by the electric field of the terahertz pulse was lock-in detected. Therefore, the induced photocurrent, which depends on both amplitude and phase of terahertz radiation, can be obtained by varying the optical delay line.

In THz-TDS, wave form of irradiated pulse electric field (ranging within a few picoseconds) is directly measured in time domain with and without the specimen. Typical example of measured terahertz wave form was indicated in Fig. 2.5. They are converted into the frequency domain via the fast Fourier transformation (FFT), and

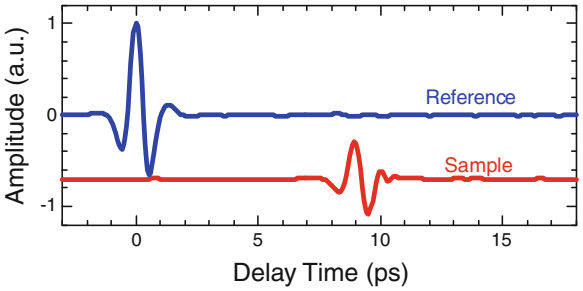

Fig. 2.5 Typical example of the measured terahertz wave form in time-domain with and without the specimen. The amplitude of the transmitted terahertz wave form with the sample was vertically offset for clarity. (Adapted with permission from [5], ©2008 APS)

the spectra of complex transmission constant (t) is deduced using the relationship $t = E^{\omega}_{\text{sample}}/E^{\omega}_{\text{ref}}$. Here, we can avoid the effect of multiple reflections and resultant interference by restricting the time range of FFT. Obtained t is further converted into complex refractive index $n = \sqrt{\epsilon\mu}$ using the following relationship;

$$t = \frac{2\mu}{n+\mu}\frac{2n}{n+\mu}\exp\left[-i\frac{\omega}{c}d(n-1)\right], \tag{2.11}$$

where ϵ, μ, d, ω, and c represent the complex dielectric constant, complex magnetic permeability, sample thickness, frequency of light, and velocity of light, respectively. To numerically solve Eq. (2.11), we approximate the pre-exponential factor by $4n/(n+1)^2$ assuming $\mu \simeq 1$ unless otherwise noted. As shown later, this approximation hardly affects the obtained n (or $\epsilon\mu$) spectrum (see "Electromagnon in the Paraelectric Collinear Spin State ").

References

1. Zhao TR, Hasegawa M, Takei H (1996) Crystal growth and characterization of cuprous ferrite ($CuFeO_2$). J Cryst Growth 166:408
2. Park S, Choi YJ, Zhang CL, Cheong S-W (2007) Ferroelectricity in an $S = 1/2$ chain cuprate. Phys Rev Lett 98:057601
3. Maljuk A, Kulakov AB, Sofin M, Capogna L, Strempfer J, Lin CT, Jansen M, Keimer B (2004) Flux-growth and characterization of $NaCu_2O_2$ single crystals. J Cryst Growth 263:338
4. Physical Property Measurement System Heat Capacity Option User's Manual, Quantum Design Inc
5. Kida N, Ikebe Y, Takahashi Y, He JP, Kaneko Y, Yamasaki Y, Shimano R, Arima T, Nagaosa N, Tokura Y (2008) Electrically driven spin excitation in the ferroelectric magnet $DyMnO_3$. Phys Rev B 78:104414

http://www.springer.com/978-4-431-54090-8

Magnetoelectric Response in Low-Dimensional Frustrated Spin Systems

Seki, S.

2012, XII, 112 p., Hardcover
ISBN: 978-4-431-54090-8